Competing single-particle and collective behavior in ^{71}Se

A. R. Howe,[1,*] R. A. Haring-Kaye,[1] J. Döring,[2] N. R. Baker,[1] S. J. Kuhn,[3] S. L. Tabor,[4] S. R. Arora,[1] J. K. Bruckman,[5] and C. R. Hoffman[4,†]

[1]*Department of Physics and Astronomy, Ohio Wesleyan University, Delaware, Ohio 43015, USA*
[2]*Bundesamt für Strahlenschutz, D-10318 Berlin, Germany*
[3]*Department of Physics and Astronomy, Earlham College, Richmond, Indiana 47374, USA*
[4]*Department of Physics, Florida State University, Tallahassee, Florida 32306, USA*
[5]*Department of Physics, Monmouth College, Monmouth, Illinois 61462, USA*

(Received 16 December 2011; revised manuscript received 29 June 2012; published 30 July 2012)

The high-spin decay of ^{71}Se was studied using the ^{54}Fe(^{23}Na,αpn) reaction at 80 MeV and the Florida State University Compton-suppressed Ge array consisting of three clover detectors and seven single-crystal detectors. Based on prompt γ-γ coincidences measured in the experiment, the known level scheme was enhanced and extended to higher spin with 19 new transitions. A band that was previously suggested to have positive parity was reassigned as the "missing" signature partner of an existing negative-parity band. Spins were assigned based on directional correlation of oriented nuclei ratios. Lifetimes of 17 excited states were measured using the Doppler-shift attenuation method. Experimental Q_t values imply an intermediate degree of collective behavior for ^{71}Se at high spin. Theoretical Q_t values determined from cranked Woods-Saxon (CWS) calculations show better agreement with the experimental ones for the positive-parity states than the negative-parity states. Shape competition and γ softness characterize the low-spin states of the lowest positive- and negative-parity bands based on the CWS calculations. At high spin, triaxial shapes with $\gamma > 0^\circ$ are predicted.

DOI: 10.1103/PhysRevC.86.014328 PACS number(s): 21.10.Tg, 23.20.Lv, 25.70.Hi, 27.50.+e

I. INTRODUCTION

The region of deformed nuclei near mass $A = 70$ has been termed the "Wild West" [1] since the structural properties of these nuclei are not as well behaved as those of the heavier deformed ones. Their collective properties change more quickly with spin and nucleon number, due in part to the smaller number of particles and lower level density available to both the valence protons and neutrons, which are filling the same orbitals in the f-p-g shell. Large shell gaps in the Nilsson single-particle energy spectrum for both proton number Z and neutron number N near 34–38 at both prolate and oblate deformation also result in strong shape competitions and rapid shape changes. These nuclei thus provide an ideal laboratory for exploring the competition between the single-particle and collective degrees of freedom.

The light $Z = 34$ Se isotopes have provided both opportunities and challenges to probe the interplay between single-particle and collective behavior. The even-even isotopes have proven to be both a popular and fertile testing ground for shape coexistence (see, for example, Refs. [2–7]), and several groups have proposed oblate ground-state configurations [4,6,8] that may persist to higher spin [4]. Other researchers have challenged the notion of oblate-deformed ground states [9,10], however, leaving this issue as an open question in these nuclei. Regardless of the interpretation of the ground-state configurations, most $N \approx Z$ Se nuclei are expected to be good candidates for oblate deformation at low spin, but then quickly transition to prolate- or triaxial-deformed shapes with increasing spin.

The neighboring odd-mass Se nuclei provide some of the clearest evidence for the rapidly changing collective properties in this mass region. For example, the level schemes of ^{69}Se [11] and ^{73}Se [12,13] show stark differences in the organization of their low-lying yrast negative-parity states. These states appear to be dominated by single-particle excitations in ^{69}Se, having irregular spacings which do not follow a rotational pattern. Collective excitations only appear to become important above an excitation energy of about 3 MeV. In contrast, the very regular, strongly coupled negative-parity yrast bands identified in ^{73}Se point to a different picture of highly collective behavior that persists throughout the observed spin range, supported by an average measured transition quadrupole moment $|Q_t| = 3.3\ e\,$b in these bands below the first band crossing [13]. Coexisting oblate and prolate shapes were associated with the structures found in both nuclei, and triaxiality was determined to be an important parameter used to describe the features of the low-lying yrast and near-yrast positive-parity bands in ^{69}Se [11].

The ^{71}Se nucleus, lying intermediate between ^{69}Se and ^{73}Se, represents a transitional case and thus might be expected to show strong competition between single-particle and collective behavior. So far, however, the available information on this nucleus is limited compared to many of its neighbors and is sometimes inconsistent with the systematics that have emerged from other studies in this region. Six low-lying states were established from the β^+ + electron capture decay of ^{71}Br [14], but their spins and parities were only suggestions based on a comparison with the low-lying level schemes of the closest $N = 37$ isotones ^{67}Zn [15,16] and ^{69}Ge [15,17].

*Present address: Department of Astrophysical Sciences, Princeton University, Princeton, New Jersey 08544, USA.
†Present address: Physics Division, Argonne National Laboratory, Argonne, Illinois 60439, USA.

The first high-spin level scheme was proposed using neutron-gated γ spectroscopy following the ^{58}Ni(^{16}O, $2pn$) heavy-ion reaction [18], the details of which are given in Ref. [19]. This decay scheme was later enhanced to include the unfavored signature partner of the yrast positive-parity band using charged-particle, neutron, and recoil mass selectivity with the same reaction [20]. However, both studies observed only a single negative-parity band structure (with signature $\alpha = -\frac{1}{2}$) based on a $\frac{7}{2}^-$ state at 1041 keV. The lack of additional high-spin negative-parity states would be very unusual in a region where several single-particle states with negative parity lie near the Fermi surface and would make ^{71}Se very different from its neighbors, regardless of its degree of collectivity. In addition, a band suggested to have positive parity was shown by both works to become yrast above an excitation energy of about 2.3 MeV, which is difficult to reconcile with the observation of another positive-parity sequence having the same spins but which is much more strongly populated. An important goal of the present work was thus to reexamine the level scheme of ^{71}Se to resolve these issues and to expand the level scheme to as high a spin as possible.

Although the lifetimes of eight high-spin excited states (including an upper limit placed on one state) have been measured previously [18], they do not extend to the band-crossing regions in any of the observed band structures. Thus another important goal of this work was to measure the mean lifetimes of as many higher-lying states as possible using the Doppler-shift attenuation method (DSAM). The determination of lifetimes then allowed for the calculation of transition strengths and transition quadrupole moments and a better picture of the degree of collectivity in ^{71}Se.

II. EXPERIMENTAL TECHNIQUES

High-spin states in ^{71}Se were produced following the ^{54}Fe(^{23}Na,αpn) fusion-evaporation reaction at a beam energy of 80 MeV using the John D. Fox superconducting accelerator at Florida State University (FSU). A 14 mg/cm^2 ^{54}Fe target, thick enough to stop all recoiling nuclei, was used to facilitate the application of the DSAM.

For this experiment, the FSU γ-detector array consisted of ten Compton-suppressed Ge detectors: three clover detectors and two single-crystal detectors placed at 90° relative to the beam direction, two single-crystal detectors placed at 35°, and three more placed at 145°. Approximately 4.6×10^8 prompt γ-ray coincidences (with each coincident event being measured within a time window of 100 ns) were recorded by the detectors and sorted into γ-γ coincidence matrices with a dispersion of either 0.4 or 0.7 keV/channel. Both the sorting and analysis of the γ-ray spectra were performed using GNUSCOPE, a γ-spectrum analysis software package developed at FSU [21,22].

The γ-ray coincidences used to verify and enhance the published level schemes were investigated mostly with background-subtracted spectra projected from matrices of coincidences among the 90° detectors, in order to minimize Doppler shifting. For the DSAM lifetime analysis, Doppler-shifted line shapes measured at 35° (145°) were obtained from background-subtracted spectra projected from matrices consisting of coincidence events between 35° (145°) detectors and 90° detectors. The choice of analyzing 35° and 145° spectra measured from coincidences with only the 90° detectors took advantage of the enhanced detection efficiency at 90° in the FSU array, and it seemed to provide the best balance between sufficient statistics and line-shape purity, even allowing for Doppler broadening as necessary when gating. Approximately 6.4×10^7 (9.2×10^7) coincidence pairs were collected in the 35° (145°) versus 90° detector matrix.

Transition energies were determined by measuring the line centroids for the transitions in as many clean gates as possible in the 90° coincidence spectra and taking a weighted average (based on individual uncertainties). Intensities for each transition were determined by gating on selected sets of transitions seen in coincidence with the entire positive- or negative-parity decay sequence. To minimize the measurement uncertainty due to Doppler-shifted line shapes, the intensities were first determined at 90° and then corrected for angular distribution effects using theoretical a_2 and a_4 coefficients determined from the spin change of the transition. These coefficients were then used to deduce A_0, the angle-independent first-order term in the series of Legendre polynomials that describe the experimental intensities as a function of observation angle. Most transitions were visible in more than one set of gates, which allowed taking a weighted average (based on the individual uncertainties) of the measured individual intensities to obtain a final accepted value. All measured γ-ray energies and intensities are given in Table I.

Spin changes were measured for as many transitions in ^{71}Se as possible based on directional correlation of oriented nuclei (DCO) ratios, defined according to

$$R_{\mathrm{DCO}} = \frac{I_\gamma \text{ (at } 35^\circ, 145^\circ\text{; gated by } \gamma_{\mathrm{G}} \text{ at } 90^\circ)}{I_\gamma(\text{at } 90^\circ\text{; gated by } \gamma_{\mathrm{G}} \text{ at } 35^\circ, 145^\circ)}. \quad (1)$$

In order to increase the statistics of the DCO ratio measurement, the analysis was performed using a matrix constructed to exploit the angular symmetry of the FSU Ge array, in which both 35° and 145° detector events were sorted against only the 90° detector events. Based on the geometry of the array, if the gate γ_G represents one or more stretched electric quadrupole ($E2$) transitions, then the DCO ratios for stretched $E2$ transitions as well as for $\Delta I = 0$ transitions are expected to be approximately unity, while $\Delta I = 1$ transitions yield ratios of about 0.5 if the mixing ratio is small [23]. All DCO ratios were measured by gating on known stretched $E2$ decays. All such measurable ratios are shown in Table I and in most cases reflect weighted averages (based on the measurement uncertainty) of the results obtained from two or more $E2$ gates.

III. ^{71}Se LEVEL SCHEME

The level scheme obtained for ^{71}Se in the present work is shown in Fig. 1. Three high-spin bands known from the most recent published level scheme [20] (shown as bands 1, 2, and 3 in Fig. 1) have been verified. In addition, some changes have been made to the known level scheme, which are discussed

TABLE I. Parent level energies, spin-parity assignments, γ-ray energies, relative intensities (A_0), DCO ratios (R_{DCO}), and multipolarities (σL) associated with the transitions assigned to ^{71}Se in this work.

E_x (keV)	I_i^π	I_f^π	E_γ (keV)	A_0	R_{DCO}	σL
171.7	$\frac{3}{2}^-$	$\frac{1}{2}^-$	122.9(3)	5(2)	0.45(16)	$M1/E2$
		$\frac{5}{2}^-$	171.7(3)	6(2)	0.65(13)	$M1/E2$
260.5	$\frac{9}{2}^+$	$\frac{5}{2}^-$	260.5[a]			$M2$
282.4	$\frac{3}{2}^-$	$\frac{1}{2}^-$	233.9(1)	12(2)	0.62(3)	$M1/E2$
		$\frac{5}{2}^-$	282.4(3)	6(2)	0.90(24)	$M1/E2$
756.9	$\frac{5}{2}^-$	$\frac{3}{2}^-$	474.5(6)	1.4(3)	0.56(38)	$M1/E2$
		$\frac{5}{2}^-$	756.9(6)	2.4(4)	1.13(44)	$M1/E2$
797.1	$\frac{5}{2}^-$	$\frac{5}{2}^-$	797.1(5)	4(2)	0.94(28)	$M1/E2$
1040.6	$\frac{7}{2}^-$	$\frac{3}{2}^-$	758.2(1)	17(3)	1.00(10)	$E2$
		$\frac{3}{2}^-$	868.9(8)	3(1)		$E2$
		$\frac{5}{2}^-$	1040.6(4)	23(4)	0.91(10)	$M1/E2$
1154.6	$\frac{11}{2}^+$	$\frac{9}{2}^+$	894.1(3)	10(2)		$M1/E2$
1233.0	$\frac{9}{2}^-$	$\frac{5}{2}^-$	1233.0(4)	16(3)	1.01(10)	$E2$
1297.8	$\frac{13}{2}^+$	$\frac{9}{2}^+$	1037.3(3)	100[b]	1.17(6)	$E2$
		$\frac{11}{2}^+$	143.2(7)	0.9(5)		$M1/E2$
1378.7	$\frac{9}{2}^-$	$\frac{5}{2}^-$	581.6(5)	2.4(5)	0.97(31)	$E2$
		$\frac{5}{2}^-$	621.8(5)	2.8(6)	0.85(19)	$E2$
		$\frac{5}{2}^-$	1378.7(4)	8(3)	0.92(32)	$E2$
1680.7	$\frac{11}{2}^-$	$\frac{7}{2}^-$	640.1(4)	44(3)	0.99(13)	$E2$
2066.2	$\frac{13}{2}^-$	$\frac{9}{2}^-$	687.5(2)	7(1)	1.06(20)	$E2$
		$\frac{9}{2}^-$	833.2(3)	14(2)	1.08(10)	$E2$
2417.9	$(\frac{15}{2}^+)$	$\frac{13}{2}^+$	1120.1(5)	9(2)		$(M1/E2)$
		$\frac{11}{2}^+$	1263.3(6)	8(2)		$(E2)$
2448.3	$\frac{17}{2}^+$	$\frac{13}{2}^+$	1150.5(1)	89(6)	0.72(4)	$E2$
2481.6	$\frac{15}{2}^-$	$\frac{11}{2}^-$	800.9(3)	40(3)	0.86(16)	$E2$
2975.8	$\frac{17}{2}^-$	$\frac{13}{2}^-$	909.6(2)	25(2)	0.87(25)	$E2$
3323.3	$\frac{17}{2}^{(-)}$	$\frac{15}{2}^-$	841.7(5)	4.5(7)	0.49(6)	$(M1/E2)$
3427.1	$\frac{19}{2}^-$	$\frac{15}{2}^-$	945.5(3)	34(5)	0.80(25)	$E2$
3451.5	$(\frac{19}{2}^+)$	$\frac{17}{2}^+$	1003.2(4)	11(2)		$(M1/E2)$
		$(\frac{15}{2}^+)$	1033.6(4)	10(4)	0.83(20)	$(E2)$
3521.4	$\frac{19}{2}^{(-)}$	$\frac{17}{2}^+$	1073.1(4)	13(2)	0.47(9)	$(E1)$
		$\frac{17}{2}^{(-)}$	198.1(4)	1.1(3)		$(M1/E2)$
3635.2	$\frac{21}{2}^+$	$\frac{17}{2}^+$	1186.9(3)	63(7)	1.29(45)	$E2$
3989.1	$\frac{21}{2}^{(-)}$	$\frac{19}{2}^{(-)}$	467.7(2)	8(2)		$(M1/E2)$
		$\frac{19}{2}^-$	562.0(4)	4(1)	0.50(9)	$(M1/E2)$
		$\frac{17}{2}^{(-)}$	665.8(2)	3(1)		$(E2)$
		$\frac{17}{2}^-$	1013.3(9)	3(2)		$(E2)$
4039.4	$(\frac{21}{2}^-)$	$\frac{17}{2}^-$	1063.6(2)	21(7)		$(E2)$
4254.3	$(\frac{23}{2}^-)$	$\frac{21}{2}^{(-)}$	265.2(4)	2.3(11)	0.67(38)	$(M1/E2)$
		$\frac{19}{2}^{(-)}$	732.9(6)	3(1)		$(E2)$
4497.2	$(\frac{23}{2}^+)$	$\frac{21}{2}^+$	862.0(10)	8(3)		$(M1/E2)$
		$(\frac{19}{2}^+)$	1045.7(7)	19(3)	0.75(26)	$(E2)$
4504.8	$\frac{23}{2}^-$	$\frac{19}{2}^-$	1077.7(5)	15(2)	1.25(29)	$E2$
4834.4	$(\frac{25}{2}^+)$	$(\frac{23}{2}^+)$	337.2(6)	2.3(15)		$(M1/E2)$
		$\frac{21}{2}^+$	1199.2(10)	36(9)		$(E2)$
5240.3	$(\frac{25}{2}^-)$	$(\frac{21}{2}^-)$	1200.9(10)	6(2)		$(E2)$
5645.5	$(\frac{27}{2}^-)$	$\frac{23}{2}^-$	1140.7(1)	7(2)		$(E2)$
5686.8	$(\frac{27}{2}^+)$	$(\frac{23}{2}^+)$	1189.6(8)	16(5)		$(E2)$
6036.4	$(\frac{29}{2}^+)$	$(\frac{25}{2}^+)$	1202.0(10)	17(4)		$(E2)$
6340.5	$(\frac{29}{2}^+)$	$(\frac{25}{2}^+)$	1506.1(3)	4(2)		$(E2)$
		$(\frac{27}{2}^+)$	653.7(3)	4(1)		$(M1/E2)$
6947.5	$(\frac{31}{2}^-)$	$(\frac{27}{2}^-)$	1302.0(8)	6(3)		$(E2)$
7375.6	$(\frac{33}{2}^+)$	$(\frac{29}{2}^+)$	1339.2(10)	12(7)		$(E2)$

[a]From Ref. [18].
[b]Intensities have been normalized to this transition.

below. In general, the level scheme construction is based on γ-γ coincidence relations and relative γ-ray intensities, and to a lesser degree on DCO ratios and effective lifetime measurements.

A. Negative-parity states

Most of the low-lying negative-parity states are known from the β^+ decay of ^{71}Br [14]. At that time, a firm spin-parity assignment of $I^\pi = \frac{5}{2}^-$ was already established for the ground state [24], and the first excited state was strongly suggested to have $I^\pi = \frac{1}{2}^-$ based on the noncollective, pure $E2$ character of the 48.8-keV transition [14]. Suggested spins and parities of other low-lying states arose from a comparison with the low-spin level schemes of the $N = 37$ isotones ^{67}Zn [15,16] and ^{69}Ge [15,17]. As in ^{67}Zn and ^{69}Ge, these states were interpreted either as single-particle states arising from the quasineutron occupation of valence orbitals in the f-p-g shell or as configurations originating from coupling the same single-particle states to vibrational states in ^{70}Se [14]. All of the low-lying negative-parity states observed in Ref. [14] were verified in this work.

One high-spin negative-parity band showing regular rotational spacings had been established above a $\frac{7}{2}^-$ state at 1040.6 keV [18], which was later verified [20]. The placement of this band was based on the decay of the $\frac{7}{2}^-$ state through a 1040.6-keV transition to the ground state and a 758.3-keV transition to the $\frac{3}{2}^-$ state at 282.4 keV. We have verified this structure and extended it to a $(\frac{31}{2}^-)$ state at 6947.5 keV (indicated as band 3 in Fig. 1). Figure 2 shows a portion of the background-corrected γ-ray spectrum measured in coincidence with the 640.1- and 800.9-keV transitions in band 3.

Other negative-parity bands have been conspicuously missing from all previous level schemes, despite the fact that multiple negative-parity bands are common in other neighboring nuclei. However, the existing high-spin level schemes [18,20] indicate a band that could be misplaced and/or misidentified as a positive-parity band. This band was built on a pair of transitions with energies of 1233.0 and 1378.8 keV

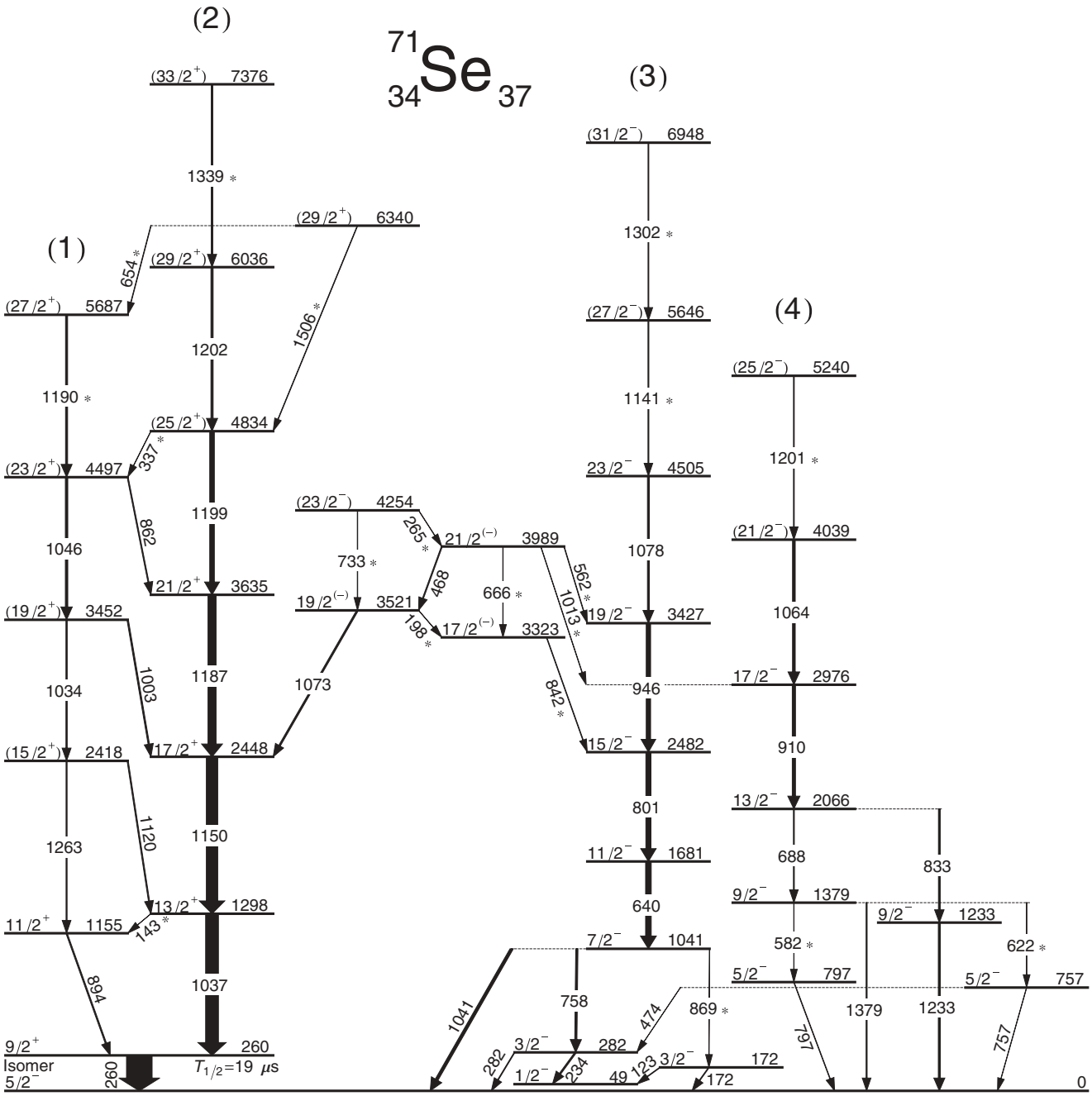

FIG. 1. Partial level scheme of ^{71}Se deduced from the present work. The 48.8-keV decay of the first excited state [14] was not observed in this work and is not shown in the figure. Transitions introduced in this work are marked with an asterisk. The arbitrary labels above each decay sequence are included to facilitate the discussion in the text.

and placed as feeding into the $\frac{9}{2}^+$ state at 260.5 keV. Since this level is an isomer with a half-life ($T_{1/2} = 19$ μs [14]) that lies well outside the coincidence timing window used in our experiment (100 ns), direct evidence for this placement could not be confirmed or refuted by simply looking for coincidences with the 260.5-keV decay of the isomer [14]. However, new evidence (discussed in detail below) has emerged which strongly suggests that the 1233- and 1379-keV transitions feed directly to the ground state, with the states above them belonging to the unfavored signature of the most strongly populated negative-parity band (shown as band 4 in Fig. 1).

The previous suggestion of positive parity for this band, with two ($\frac{13}{2}^+$) levels at the bottom, results in all of the higher levels in the band sharing the same spins as states in the yrast positive-parity band (band 2 in Fig. 1), yet lying relatively lower in energy. This is highly unlikely given the relative population of the states in these two bands. Also, the existing placement of this band was "floating" in the sense that there were

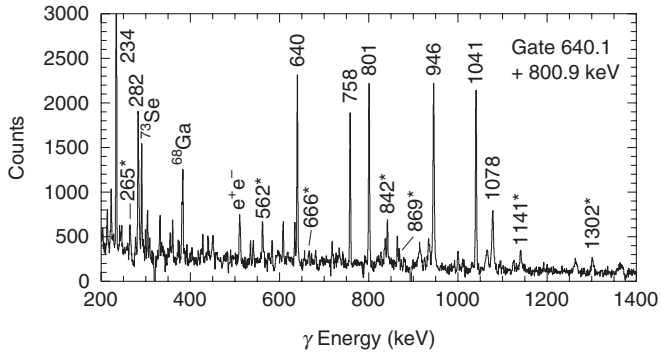

FIG. 2. A portion of the 90° background-corrected spectrum obtained by summing gates on the 640.1- and 800.9-keV γ rays in band 3. Peak energies labeled with asterisks indicate transitions assigned to ^{71}Se in this work.

no observed decays out of this band to other known states that would firmly establish the energies of the states in this band. However, our γ-γ coincidence data clearly show coincidences between transitions within this band and those between low-lying negative-parity states, as demonstrated by the spectrum shown in Fig. 3. A search for transitions that connect states in this band with the low-lying negative-parity states revealed a 621.8-keV transition in coincidence with the known 756.9-keV line [14], along with a 581.6-keV γ ray in coincidence with a 797.1-keV transition that had already been tentatively placed from the β^+ decay of ^{71}Br [14]. Both of these decay sequences establish a new level at 1378.7 keV, which matches the measured energy of the 1379-keV transition within measurement uncertainty. This strongly suggests that the 1379-keV γ ray represents a decay to the ground state, rather than to the $\frac{9}{2}^+$ isomer, and thus allows for a new placement of the associated band above this transition (band 4 in Fig. 1).

Both the 1233.0- and 1378.7-keV transitions show DCO ratios near unity when gating on higher-lying $E2$ transitions in band 4, consistent with stretched $E2$ radiation and supporting a spin-parity assignment of $I^\pi = \frac{9}{2}^-$ for both the 1233.0- and 1378.7-keV states. A similar pattern is observed in other nuclei with $\frac{5}{2}^-$ ground states such as ^{69}Se [11], ^{69}Ge [25], and

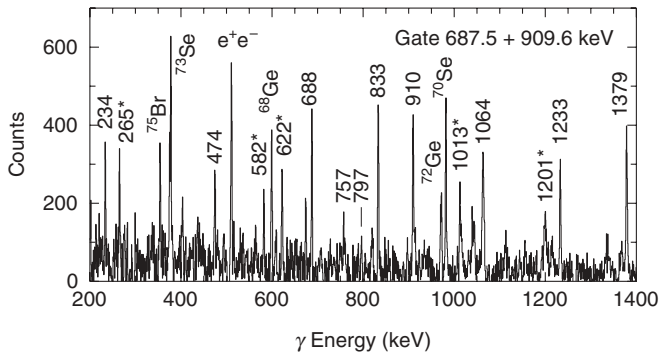

FIG. 3. A portion of the 90° background-corrected spectrum obtained by summing gates on the 687.5- and 909.6-keV γ rays in band 4. Peak energies labeled with asterisks indicate transitions assigned to ^{71}Se in this work.

^{71}As [26–28], where the most strongly populated $\frac{13}{2}^-$ state shows two competing $E2$ decays to two relatively closely spaced $\frac{9}{2}^-$ states. The 581.6- and 621.8-keV decay branches of the 1378.7-keV state lead to respective states at 797.1 and 756.9 keV, which likely correspond to the 796.4- and 756.7-keV states observed in Ref. [14] (although the 796.4-keV state was only tentatively placed). Both of these transitions show DCO ratios consistent with $E2$ decays, establishing a spin-parity of $\frac{5}{2}^-$ for both the 756.9- and 797.1-keV states. This assignment is also consistent with the measured DCO ratios of the decays of these states (see Table I). The 797.1-keV state was taken as the bandhead of band 4 since this choice leads to a somewhat smoother behavior of the kinematic moments of inertia for this band at low frequencies (see Sec. V A). Other suggested spin-parity assignments in band 4 were made by assuming $E2$ character for the intraband transitions. This band sequence has also been extended by one additional transition above what had already been observed [18,20].

We also observed a set of high-lying states that appear to be longer lived than other states at similar excitation energy since their associated decays do not show Doppler shifting. Two of these states (at 3521.4 and 3989.1 keV) were observed previously [18] but later removed from the high-spin decay scheme [20]. Two other states within this cluster (at 3323.3 and 4254.3 keV) were firmly established from the γ-ray coincidence relations. A state at 4525.5 keV, observed in Ref. [18], could not be confirmed in this work. It is very likely that the 1003.9-keV decay associated with this proposed state corresponds to the $(\frac{19}{2}^+) \rightarrow \frac{17}{2}^+$ transition first observed in Ref. [20] and verified in this study.

The measured DCO ratios of the 841.7-, 1073.1-, and 562.0-keV transitions establish spins for the 3323.3-, 3521.4-, and 3989.1-keV states, respectively, while the spin of the 4254.3-keV state remains tentative due to the rather large uncertainty in the measured DCO ratio of the 265.2-keV transition. Negative parity is suggested for these states based on their strong resemblance with states in other neighboring odd-A nuclei that have similar spins, excitation energies, and decays to more strongly populated structures (see Sec. V D).

B. Positive-parity states

Two low-lying positive-parity states were identified from the β^+ decay of ^{71}Br [14]. The lowest one at 260.5 keV was assumed to be a $g_{9/2}$ neutron single-particle state ($I^\pi = \frac{9}{2}^+$) based on the measured $B(M2)$ transition strength [0.078(13) W.u.] of the 260.5-keV decay to the ground state and its consistency with those of similar transitions in ^{67}Zn and ^{69}Ge. A $\frac{5}{2}^+$ state was also observed at 647.6 keV, suggested to arise from the coupling of a $g_{9/2}$ neutron to the 2_1^+ state in ^{70}Se, although this state was not observed in the present study.

As is the case with several other odd-A nuclei in this mass region, the $\frac{9}{2}^+$ state serves as the bandhead of the yrast positive-parity band in ^{71}Se (band 2 in Fig. 1). It was established up to a 6035.3-keV state [18], which was later confirmed [20]. The much weaker signature $\alpha = -\frac{1}{2}$ partner band (band 1 in Fig. 1) was first discovered in the most recent published work [20].

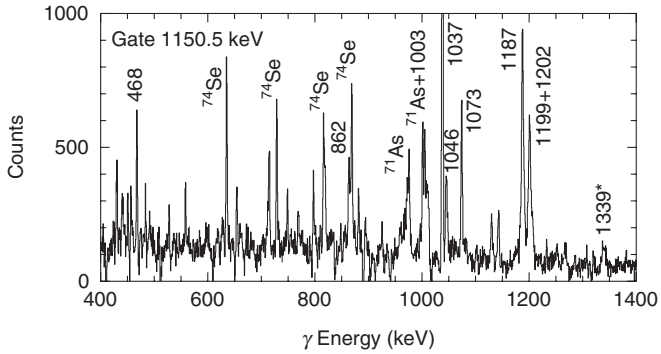

FIG. 4. A portion of the 90° background-corrected spectrum obtained by gating on the 1150.5-keV γ ray in band 2. Peak energies labeled with asterisks indicate transitions assigned to ^{71}Se in this work.

In the current work we have verified the existing signature-partner bands, extended the $\alpha = +\frac{1}{2}$ sequence to a $(\frac{33}{2}^+)$ state at 7375.6 keV, and found two new linking transitions between bands 1 and 2 (see Fig. 1). In addition, two new states at 5686.8 and 6340.5 keV were established from the γ-γ coincidence relationships. Figure 4 shows several transitions associated with bands 1 and 2 through their observed coincidences with the 1150.5-keV decay, as well as some transitions associated with a high-lying negative-parity structure (see Sec. III A).

IV. LIFETIME MEASUREMENTS AND TRANSITION STRENGTHS

Lifetimes of 17 excited states were measured by applying the DSAM to the experimental line shapes of coincident γ rays detected at 35° and 145°. A comparison between the decay time of the recoiling nuclei and the slowing down in a thick target was carried out using the simulation code FITS [23], which integrates over the thickness of the target and accounts for evaporation of charged particles by determining a Gaussian distribution of recoil velocities (with a width that is 10% of the kinematic mean) at the time of decay. It corrects for direct feeding from up to four known higher-lying states and side feeding from one unknown state, as well as for finite detector solid angle and resolution and the changing (energy-dependent) reaction cross sections due to the beam slowing down through the target. The nuclear and electronic stopping powers were obtained from the SRIM-2008 software [29].

A set of theoretical line shapes was produced based on possible lifetimes of the state of interest and compared with the measured Doppler-shifted spectrum at 35° and 145° to find the best fit (representing the lowest χ^2 when compared to the experimental spectrum), which was taken as the lifetime of that state. The limits of uncertainty in the individual lifetimes were taken to be the lifetime values above and below the best-fit value that increased the minimum χ^2 value by one unit, and thus they represent an estimate of the statistical uncertainties (one-standard deviation) in the lifetime measurements [30]. The accepted lifetime values were determined from a weighted average (based on the measured uncertainties) of the individual lifetimes whenever measurements were possible at both angles (see Table II). If a measurement could only be performed at one angle, then the accepted lifetime (and its uncertainty) came directly from the measurement at that angle. The uncertainties in the accepted lifetimes representing a weighted average were deduced from the reciprocal square root of the sum of the individual weights, with each individual weight given by the reciprocal square of the measurement uncertainty [31].

Effective lifetimes, which do not include feeding corrections, were first determined for each line shape with adequate statistics. Whenever possible, an accepted effective lifetime of each state was determined from the weighted average (based on the individual uncertainties) of the results obtained from each of the two detector angles. All line shapes for which the feeding was known were then refit with feeding corrections. The feeding corrections used the effective lifetime of the state (or possibly multiple states) immediately above and one side-feeding state to feed the state of interest.

Whenever possible, mean lifetimes were determined from spectra gated from above (GFA) the transitions of interest, eliminating the effects of side feeding. However, limited statistics often required the analysis of line shapes obtained from spectra gated from below (GFB) the transition of interest. In these situations, a side-feeding time of 0.03 ps was assumed for states near 5 MeV excitation energy, and it was assumed to increase by 0.03 ps per MeV of de-excitation. This choice is consistent with the assumptions used in other recent studies of nuclei in the mass 70–80 region (see, for example, Ref. [28]), which have been motivated by a rigorous theoretical study of side-feeding times in this mass region [32], as well as the measured results from ^{82}Sr [33] and ^{83}Y [34]. Of course, one should keep in mind that shorter (longer) side-feeding times used in the feeding corrections would result in longer (shorter) mean lifetimes. In many cases, however, the resulting mean lifetimes measured in this work were rather insensitive to the side-feeding time as long as the side-feeding intensity was small. For example, doubling the assumed side-feeding time would typically result in a $<$10% change in the resulting mean lifetime. On the other hand, modifying the feeding intensities within the range of the uncertainties in the intensities given in Table I could result in maximum changes to the mean lifetimes of about 40%. An attempt to directly measure side-feeding times in ^{71}Se through a comparison of GFA and GFB line-shape fits usually resulted in large uncertainties, indicating an insensitivity of the observed GFB line shapes to the side-feeding time.

In addition to the potential systematic uncertainty introduced by the side-feeding time and intensity, other sources of systematic uncertainty can arise primarily from the calculated stopping powers and unresolved contaminant lines. Uncertainties in the stopping powers associated with heavy-ion beams, recoils, and targets using SRIM calculations are expected to be $<$5% [35,36]. Line-shape simulations consistently indicated an increase (decrease) in the best-fit mean lifetimes of about 7% when the stopping powers were decreased (increased) by 5%. Unresolved contaminant peaks are difficult to account for in the analysis, but they could contribute to an average fractional uncertainty of about 40% based on the percent differences between individual lifetimes measured at both 35° and 145°.

TABLE II. Initial-state spins, γ-ray transition energies, mean lifetimes, electric quadrupole transition strengths $B(E2)$, and transition quadrupole moments $|Q_t|$ in ^{71}Se measured in this work. Individual mean lifetimes deduced from a DSAM analysis of line shapes measured at the indicated angles from transitions with energy E_γ are given in the same row. The accepted mean lifetimes ($\tau_{\rm acc}$) represent the weighted average (based on the uncertainties) of the measurements at 35° and 145° where results are available.

I_i^π	E_γ (keV)	$\tau_{\rm prev}$[a] (ps)	τ_{35°[b] (ps)	τ_{145°[b] (ps)	$\tau_{\rm acc}$ (ps)	$B(E2)$ (W.u.)[c]	$\lvert Q_t\rvert$ (e b)
				Band 1			
$(\frac{15}{2}^+)$	1263.3			0.39^{+11}_{-10}	0.39^{+11}_{-10}	37^{+13}_{-8}	1.63^{+26}_{-19}
$(\frac{19}{2}^+)$	1033.6			0.43^{+12}_{-9}	0.43^{+12}_{-9}	66^{+17}_{-14}	2.01^{+25}_{-23}
$(\frac{23}{2}^+)$	1045.7		<1.15[d]		<1.15[d]	>20	>1.07
				Band 2			
$\frac{13}{2}^+$	1037.3	1.30(40)	>2[e]	>2[e]	>2[e]	<19	<1.25
$\frac{17}{2}^+$	1150.5	0.77(30)	0.77^{+6}_{-5}[e]		0.77^{+6}_{-5}[e]	30(2)	1.40(5)
$\frac{21}{2}^+$	1186.9	0.58(40)	0.44(3)[e]	0.36^{+4}_{-3}[e]	0.41(2)[e]	48(2)	1.69(4)
$(\frac{25}{2}^+)$	1199.2		0.56(5)	0.35(6)	0.47(4)	38^{+4}_{-3}	1.46^{+7}_{-6}
$(\frac{29}{2}^+)$	1202.0		0.57(5)	0.52(5)	0.54(4)	34^{+3}_{-2}	1.36(5)
$(\frac{33}{2}^+)$	1339.2		<0.13[d]		<0.13[d]	>84	>2.09
				Band 3			
$\frac{15}{2}^-$	800.9	0.76(40)	>2[e]	>2[e]	>2[e]	<71	<2.24
$\frac{19}{2}^-$	945.5	<1	1.45^{+8}_{-7}	0.81^{+3}_{-4}	0.92(3)	67(2)	2.03(3)
$\frac{23}{2}^-$	1077.7		0.56^{+3}_{-2}	0.42(2)	0.48(2)	67(3)	1.95(4)
$(\frac{27}{2}^-)$	1140.7		0.78^{+8}_{-6}	0.42(6)	0.57(5)	42^{+4}_{-3}	1.52^{+7}_{-6}
$(\frac{31}{2}^-)$	1302.0		<0.33[d]	<0.14[d]	<0.24[d]	>52	>1.66
				Band 4			
$\frac{17}{2}^-$	909.6		1.88^{+31}_{-24}	1.05^{+13}_{-11}	1.18(11)	64^{+7}_{-5}	2.04^{+10}_{-9}
$(\frac{21}{2}^-)$	1063.6		0.75(3)	0.62^{+4}_{-3}	0.70(2)	49(1)	1.70(2)
$(\frac{25}{2}^-)$	1200.9			<0.24[d]	<0.24[d]	>78	>2.08

[a]From Ref. [20].
[b]Determined from spectra gated from below (GFB) the listed transition, unless otherwise noted.
[c]1 W.u. = 17.46 e^2 fm^4.
[d]Effective lifetime.
[e]Determined from spectra gated from above (GFA) the listed transition.

The results of the lifetime measurements are shown for both detector angles along with previous results from Ref. [18] in Table II. Where applicable, an accepted lifetime $\tau_{\rm acc}$, representing a weighted average of the two detector angles, has been given. An upper limit placed on a mean lifetime τ represents an effective lifetime for a state for which feeding corrections could not be made. A lower limit of 2 ps was placed on τ if the fit to the line shape of the associated parent-state decay resulted in a χ^2 value that did not converge to a minimum below $\tau = 2$ ps when feeding corrections were invoked. Three representative line-shape fits are shown in Fig. 5.

Lifetime measurements were extended for the favored signature $\alpha = +\frac{1}{2}$ positive-parity band (band 2 in Fig. 1) up to the $(\frac{33}{2}^+)$ state, for which an effective lifetime was measured. Three lifetimes were also measured in the unfavored $\alpha = -\frac{1}{2}$ positive-parity band (band 1 in Fig. 1) for the first time, although weaker statistics led to rather large uncertainties in these measured values. Similarly, lifetimes were measured in the favored $\alpha = -\frac{1}{2}$ negative-parity band (band 3 in Fig. 1) up to an effective lifetime for the $(\frac{31}{2}^-)$ state. Lifetimes were measured for three states in the reassigned, unfavored $\alpha = -\frac{1}{2}$ negative-parity band (band 4 in Fig. 1) for the first time, including an effective lifetime for the $(\frac{25}{2}^-)$ state.

A simultaneous fit was performed to the 1199.2- and 1202.0-keV doublet to decompose their individual GFB line shapes and extract lifetimes for the $(\frac{25}{2}^+)$ and $(\frac{29}{2}^+)$ states, respectively. A modified version of FITS [37] was used to fit the two overlapping line shapes simultaneously, with the theoretical line shapes scaled by the intensity of each transition.

When performing GFB fits to the line shape of the 945.5-keV transition in band 3 (an example of which is shown in Fig. 5), it was clear that a long-lived feeding component was contributing to the observed line shape, probably due at least in part to feeding from the newly observed $\frac{21}{2}^{(-)}$ state at 3989.1 keV (see Fig. 1). The lifetime of this $\frac{21}{2}^{(-)}$ state was clearly too long to measure using the DSAM. However, a similar high-lying, relatively long-lived $\frac{21}{2}^{(-)}$ state exists in

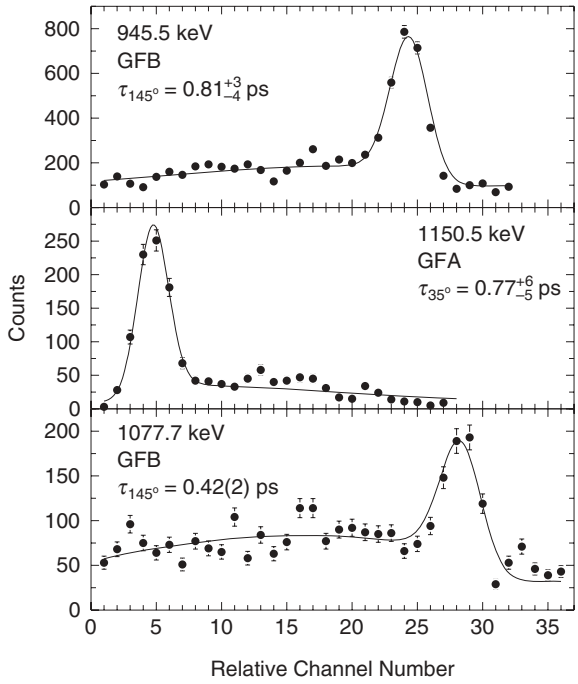

FIG. 5. Fits to the 145° line shapes of the 945.5- and 1077.7-keV transitions in band 3, as well as the 35° line shape of the 1150.5-keV transition in band 2. Line shapes that were determined by gating from below (GFB) and gating from above (GFA) the given transition are indicated.

^{71}As [26] with a mean lifetime of 540(100) ps [26,38]. Thus we approximated the effect of direct feeding from the $\frac{21}{2}^{(-)}$ state in our GFB fits to the 945.5-keV transition by assuming a feeding lifetime of 540 ps, which resulted in a better fit (smaller χ^2) to the experimental line shape than if no long-lived feeding component was included. The measured lifetime of the $\frac{19}{2}^{-}$ parent state, however, was rather insensitive to the assumed value of this feeding lifetime since the direct feeding from the $\frac{21}{2}^{(-)}$ state accounted for only 13% of the total feeding intensity into the $\frac{19}{2}^{-}$ state. Of course, a GFA fit to the 945.5-keV line shape would eliminate the need for this approximation, but this was not possible due to limited statistics. The difficulty in performing such a GFA fit was exacerbated by the fact that a gate on the transition just above the 945.5-keV decay in band 3 (1077.7 keV) includes to some extent the intense 1075.4-keV line in ^{71}As [26–28], which shows strong coincidences with the 943.5-keV overlapping contaminant peak.

By considering the states for which mean lifetimes had been previously measured [18], our results for the $\frac{17}{2}^{+}$ and $\frac{21}{2}^{+}$ states in band 2 and the $\frac{19}{2}^{-}$ state in band 3 agree with Ref. [18] (see Table II). Two others (those of the $\frac{7}{2}^{-}$ and $\frac{11}{2}^{-}$ states in band 3) were too long to independently verify using the DSAM. In the two cases where disagreement was noted (the $\frac{13}{2}^{+}$ state in band 2 and the $\frac{15}{2}^{-}$ state in band 3), we have taken our lower limit of 2 ps as the accepted mean lifetime for these states since these were determined from a GFA analysis, which would remove any uncertainties that may have been involved with the side-feeding corrections used previously.

Reduced electric quadrupole transition strengths $B(E2)$ were determined for the $E2$ transitions from the accepted lifetime of the associated parent state. These were then used to calculate transition quadrupole moments $|Q_t|$ from the rotational model according to

$$Q_t^2 = \frac{16\pi}{5}\langle I\,K\,20|I-2K\rangle^{-2}B(E2, I \to I-2). \quad (2)$$

An effective value for the spin projection quantum number of $K = \frac{5}{2}$ was used for all bands in ^{71}Se. The $B(E2)$ and $|Q_t|$ values inferred from the lifetime measurements are given in Table II.

V. DISCUSSION

Most of the known [20] band structures in ^{71}Se have been extended to higher spin in this study and indicate at least a moderate degree of collectivity based on the results of the lifetime measurements (see Table II). Thus the observed bands were interpreted within the context of the cranked shell model (CSM), which allowed for an investigation of the first quasiproton alignment in the lowest positive- and negative-parity bands (bands 2 and 3 in Fig. 1). Now that lifetime measurements are available for the first time in the unfavored positive- and negative-parity bands (bands 1 and 4 in Fig. 1), and those for bands 2 and 3 have been extended to higher spins, a more complete picture of the degree of collectivity could be determined for different intrinsic configurations and compared with the predictions of cranked Woods-Saxon (CWS) calculations. These comparisons also provided a test of the shapes predicted by the CWS calculations. Additionally, a quantitative determination of the degree of collectivity through the first quasiproton alignment observed in bands 2 and 3 could be performed. The results of each of these investigations are discussed separately in the sections that follow.

A. Cranked shell-model calculations

Experimental kinematic moments of inertia $J^{(1)}$ as a function of rotational frequency were extracted for bands 1–4 in ^{71}Se using the CSM applied to the level energies and spins given in Table I, and these are shown in Fig. 6. After a rather sharp increase, a clear peak is observed near $\hbar\omega = 0.59$ MeV in the $J^{(1)}$ spectrum for band 2 (filled circles in the top panel of Fig. 6), most likely indicating the first quasiproton alignment (since the first quasineutron alignment is Pauli blocked). The maximum calculated value of $J^{(1)} \approx 24\ \hbar^2$/MeV is nearly the same as that observed for band 3 (as indicated in the lower panel of Fig. 6), even though the $B(E2)$ strengths are somewhat larger in band 3 than they are in band 2 (see Table II). The $J^{(1)}$ spectrum for band 1 (open circles in the top panel of Fig. 6) shows a very different behavior compared to band 2, due to the observed energy differences between successive states in this band, which do not increase regularly with increasing excitation energy.

Negative-parity bands 3 and 4 both display $J^{(1)}$ values that gradually increase with frequency, until a plateau is observed near $\hbar\omega \approx 0.56$ MeV in the band 3 spectrum, very likely

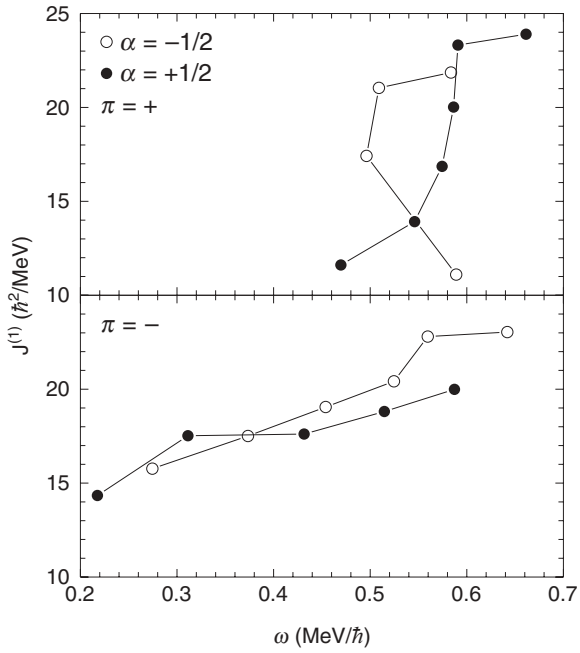

FIG. 6. Experimental kinematic moments of inertia $J^{(1)}$ as a function of rotational frequency for all four observed bands in ^{71}Se. A common value of $K = \frac{5}{2}$ was used for all bands.

indicating a quasiproton alignment in this structure. No such alignment was observed within band 4.

B. Cranked Woods-Saxon calculations

The evolution of shape and deformation with rotational frequency was investigated for band structures based on both signatures of the lowest positive- and negative-parity intrinsic configurations using the CWS approach [39]. The calculations generate a total Routhian surface (TRS) plot in the (β_2, γ) plane at discrete rotational frequencies, using a deformed Woods-Saxon potential and a short-range monopole pairing force. At each grid point, the Routhian was minimized with respect to the hexadecapole deformation β_4. Figure 7 shows six representative TRS plots resulting from these calculations for the lowest positive- and negative-parity configurations with signature $\alpha = +\frac{1}{2}$ at three rotational frequencies which span the range of those observed in this study. These calculations most likely represent bands 2 and 4 in ^{71}Se, although very similar TRS plots were obtained for the corresponding signature partner configurations with $\alpha = -\frac{1}{2}$.

The two sets of calculations show strong similarities in their behavior as a function of rotational frequency. At low rotational frequency, the calculations predict three competing shallow minima near $\gamma = 0^\circ$ and $\pm 60^\circ$, indicating a degree of γ softness that is typical of the light Se isotopes and $A \approx 70$ nuclei in general. The energy difference between each of these minima is no more than 0.09 (0.03) MeV for the positive-parity (negative-parity) states at $\hbar\omega = 0.1$ MeV. At intermediate frequencies, the near-prolate minimum appears to deepen in both configurations, while the near-oblate minimum persists only in the negative-parity states. At higher frequencies, both configurations demonstrate deeper triaxial minima with varying positive values of γ.

It could be that the collective shape changes revealed by the TRS plots in Fig. 7 represent a migration from near-oblate to near-prolate and/or triaxial shapes with increasing rotational frequency within the corresponding band structures. A similar shape progression in the positive-parity states was suggested based on a recent measurement of the magnitude and sign of the mixing ratios for some of the intraband $M1$ transitions between bands 1 and 2 [40]. It is also possible that the noncollective oblate minima observed in the negative-parity states are related to the proposed noncollective structure (see Sec. III A).

Previous determinations of optimal shape parameters β_2 and γ for bands 2 and 3 were obtained by comparing measured $B(E2)$ strengths with those predicted by asymmetric rotor plus quasiparticle model calculations [18,41]. The calculations best reproduced the experimental results when $\beta_2 = 0.2$ and $\gamma = +27^\circ$ ($\beta_2 = 0.39$ and $\gamma = +28^\circ$) were used for band 2 (3). Although these calculations do not show the dynamic shape characteristics of these bands with spin revealed by the CWS calculations, both models predict reduced collectivity overall for band 2 compared to band 3 and demonstrate the need to incorporate nonaxial shapes in the theoretical description of these bands.

C. Transition quadrupole moments

Theoretical $|Q_t|$ values were deduced from the β_2 values obtained from the TRS plots for the purpose of comparison with the experimental ones determined from Eq. (2). In order to make a proper comparison, the quadrupole deformation β_2^v of the nuclear matter distribution derived from the TRS calculations [42,43] was first related to the charge quadrupole deformation β_2^ρ derived from the $B(E2)$ strengths using

$$\beta_2^\rho = 1.1\beta_2^v. \tag{3}$$

For the case of prolate-deformed axial symmetry ($\gamma = 0^\circ$), $|Q_t|$ and β_2^ρ are related by [42]

$$Q_t(\gamma = 0^\circ) = \left| \frac{6eZr_0^2A^{2/3}}{7\pi} \left\{ \left[\beta_2^\rho + 7\sqrt{\pi/80}\right]^2 - 49\frac{\pi}{80} \right\} \right|, \tag{4}$$

with $r_0 = 1.2$ fm used in this analysis. However, in order to take triaxiality into account, the high-spin limit for the γ dependence of $|Q_t|$ was incorporated according to [44,45]

$$|Q_t| = (2/\sqrt{3})Q_t(\gamma = 0^\circ)|\cos(\gamma + 30^\circ)|. \tag{5}$$

Equation (5) implies that even moderate triaxiality with $\gamma > 0^\circ$ can substantially lower $|Q_t|$, while negative values of γ have relatively little effect until γ approaches the oblate-deformed axial limit at -60°.

The theoretical $|Q_t|$ values obtained in this fashion are compared with the experimental ones in Fig. 8. In the figure, theoretical values are included for collective minima observed in the TRS plots at both positive (solid and dotted curves) and negative (dashed and dot-dashed curves) values of γ for signatures of both the lowest positive- and negative-parity configurations available in the calculations. Theoretical values

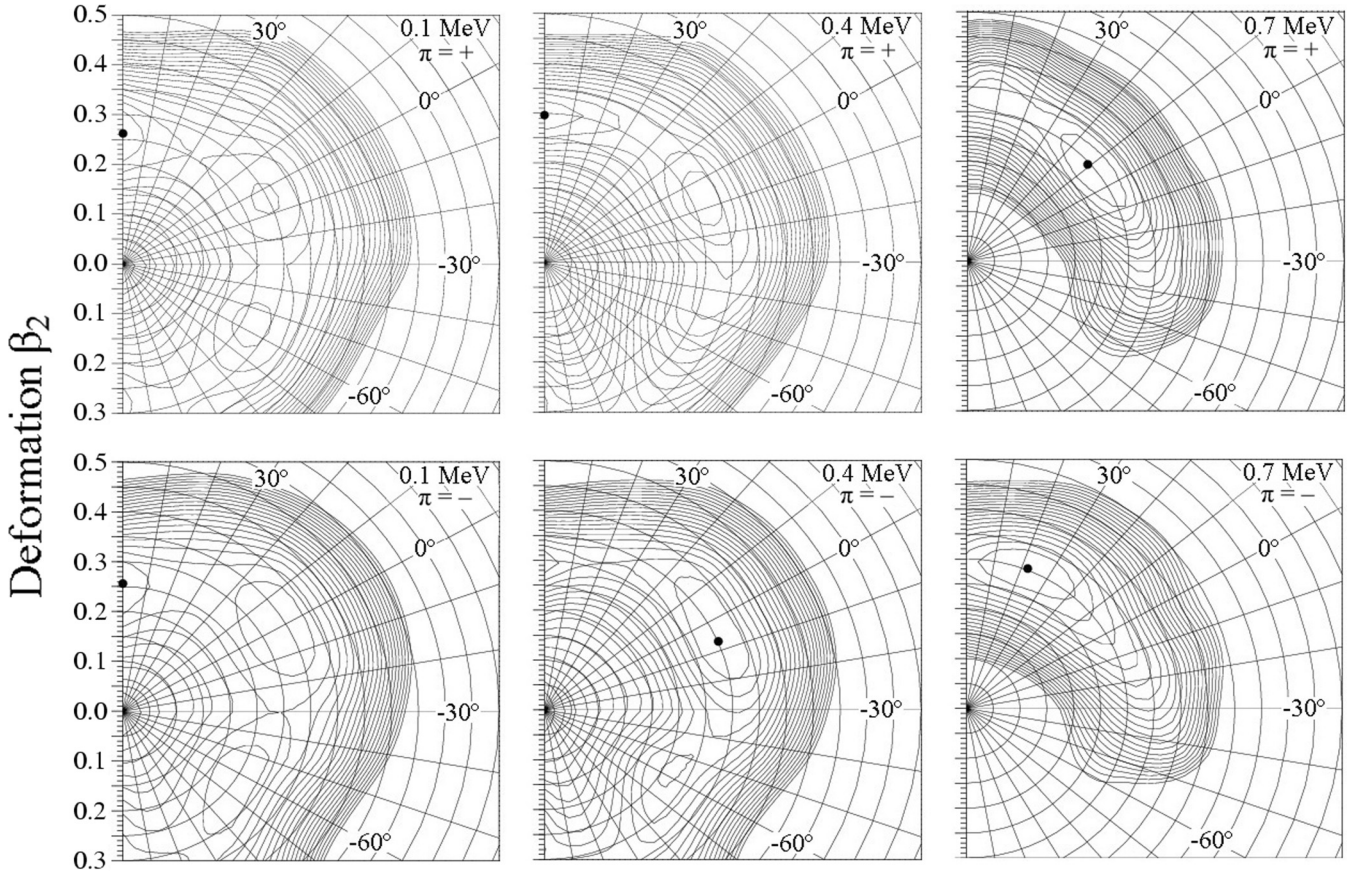

FIG. 7. Sample total Routhian surfaces in the (β_2, γ) plane for intrinsic quasiparticle configurations that most likely represent band 2 (top row) and band 4 (bottom row) in ^{71}Se at rotational frequencies of $\hbar\omega = 0.1$ (left column), 0.4 (middle column), and 0.7 MeV (right column). The spacing between contour lines is 200 keV.

corresponding to $\gamma < 0^\circ$ do not persist in the calculations above $\hbar\omega \approx 0.4$ MeV. In general, the experimental $|Q_t|$ values for the positive-parity states (top panel of Fig. 8) are well reproduced by the calculations corresponding to $\gamma > 0^\circ$. On the other hand, most of the experimental values for the negative-parity states (lower panel of Fig. 8) disagree with the predicted ones, with the experimental values being systematically larger than the theoretical ones. The downward trend in $|Q_t|$ predicted to occur for $\hbar\omega > 0.4$ MeV in the configurations with triaxial shapes is caused by increasing triaxiality at higher rotational frequency (see Fig. 7).

The experimental $|Q_t|$ values obtained for bands 1–4 in ^{71}Se are also compared with those measured within similar band structures in ^{69}Ge [25], ^{73}Se [12], and ^{73}Kr [46] in Fig. 9. The values in ^{71}Se for both positive-parity (top panel of Fig. 9) and negative-parity (bottom panel of Fig. 9) states lie intermediate between those in ^{69}Ge and those in ^{73}Se and ^{73}Kr, clearly demonstrating both the increase in collectivity as N, Z approach midshell and the transitional character of ^{71}Se compared with its neighbors.

D. Three-quasiparticle excitations

As mentioned in Sec. III A, a set of high-lying states with excitation energies in the range of about 3.3–4.3 MeV was found through the γ-γ coincidence relationships, two of which had been observed in previous work [18]. The decay pattern and high excitation energy associated with this cluster of states suggests a three-quasiparticle (3-qp) structure, although probably not one which corresponds to a crossing of the existing bands. Instead, it may be more appropriate to interpret these states as 3-qp excitations arising from the coupling of a $g_{9/2}$ neutron to known negative-parity states in the even-even ^{70}Se core [5]. Similar 3-qp structures have been found in other neighboring odd-A nuclei, including ^{69}Ge [25] and ^{71}As [26]. The analogous states in ^{71}Se show some similarities to and differences from the systematic patterns established in these cases, as will be discussed further below.

In ^{70}Se, the lowest 6^- state is at an excitation energy of 3789 keV. Taking the $g_{9/2}$ neutron excitation energy as 260 keV in ^{71}Se (i.e., the energy difference between the $\frac{9}{2}^+$ state and the ground state) and adding it to the excitation energy of the 6^- state in ^{70}Se gives 4049 keV, which is very close to the observed energy of the $\frac{21}{2}^{(-)}$ state in ^{71}Se (3989.1 keV). Similarly, the lowest 5^- state in ^{70}Se has an excitation energy of 3387 keV, which by a similar procedure would point to a $\frac{19}{2}^-$ state near 3647 keV in ^{71}Se, which is in good agreement with the observed $\frac{19}{2}^{(-)}$ state at 3521.4 keV. In this way, even the observed $(\frac{23}{2}^-)$ state at 4254.3 keV could be viewed as the

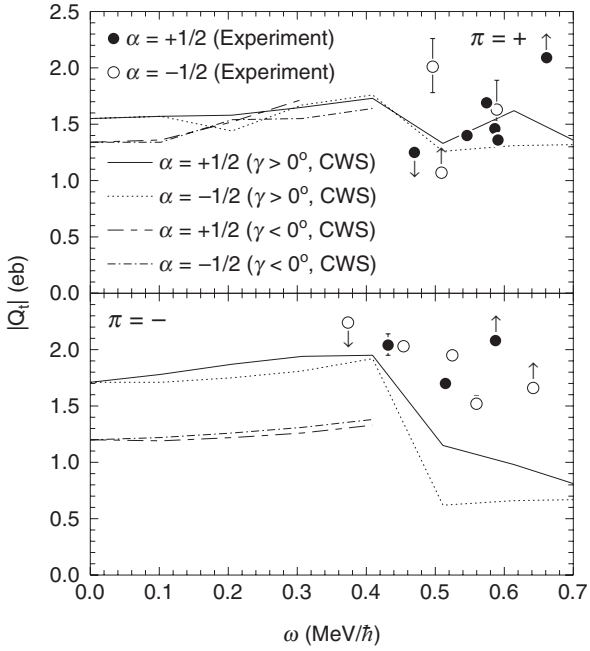

FIG. 8. Transition quadrupole moments $|Q_t|$ as a function of rotational frequency for bands 1–4 in ^{71}Se. Symbols with arrows indicate either upper or lower limits established by lifetime measurements. Some error bars are smaller than the symbol size. The solid and dotted (dashed and dot-dashed) curves represent theoretical predictions from cranked Woods-Saxon (CWS) calculations associated with TRS minima corresponding to positive (negative) values of γ, as indicated in the figure.

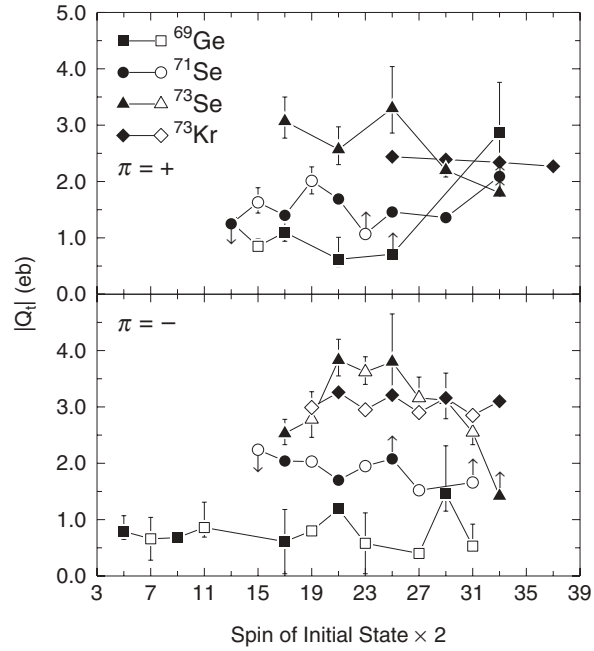

FIG. 9. Transition quadrupole moments $|Q_t|$ as a function of initial-state spin for the two lowest positive-parity (top panel) and negative-parity (bottom panel) bands in ^{69}Ge [25], ^{71}Se, ^{73}Se [12], and ^{73}Kr [46], where data are available. The ^{71}Se values reflect those measured in this work. Filled (open) symbols correspond to initial states with signature $\alpha = +1/2$ ($\alpha = -1/2$), and those with arrows indicate either upper or lower limits established by lifetime measurements. Some error bars are smaller than the symbol size.

coupling of a $g_{9/2}$ neutron to the 7^- state at 3915 keV in ^{70}Se. Similar interpretations of an unpaired $g_{9/2}$ particle coupled to its corresponding even-even core have been proposed for analogous states in ^{69}Ge [25] and ^{71}As [26].

However, some differences in the pattern of such states in ^{71}Se and those of its neighboring odd-A isotopes have also been observed. For example, in both ^{69}Ge and ^{71}As two relatively closely spaced $\frac{19}{2}^-$ states were observed, both of which decay to the yrast $\frac{17}{2}^+$ state. These states were interpreted as arising from the coupling of a $g_{9/2}$ particle to closely spaced 5^- states in the even-even core of these nuclei. Based on this simple picture, we would expect a similar structure in ^{71}Se since two closely spaced 5^- states have been observed in ^{70}Se [5]. However, only the state at 3521.4 keV could serve as a candidate for the expected pair of closely spaced $\frac{19}{2}^-$ states in ^{71}Se, although it appears to be well explained by the coupling of a $g_{9/2}$ neutron to the lowest 5^- state at 3387 keV in ^{70}Se. The lack of a second such $\frac{19}{2}^-$ state in ^{71}Se could point to different intrinsic configurations for the two 5^- states in ^{70}Se. We note also that the decays of the second, higher-lying $\frac{19}{2}^-$ state in ^{69}Ge were only very weakly observed [25]. In addition, we searched for a $\frac{15}{2}^-$ state near 2779 keV in ^{71}Se which decays to the yrast $\frac{13}{2}^+$ state based on the observed decay of a 3^- state at 2519 keV to the 2_1^+ state in ^{70}Se, but no candidate was found.

VI. SUMMARY

High-spin states in ^{71}Se were studied using the ^{54}Fe(^{23}Na,αpn) reaction at 80 MeV performed at the John D. Fox superconducting accelerator at Florida State University. The isotopically enriched ^{54}Fe target was thick enough to stop all recoils and hence allowed for the measurement of lifetimes using the Doppler-shift attenuation method. γ rays were detected in prompt coincidence using a Compton-suppressed Ge array consisting of three high-efficiency clover detectors and seven single-crystal detectors. The existing level scheme of ^{71}Se has been confirmed in part, modified to reflect a reassignment of one band, and enhanced to include 19 new transitions based on the investigation of γ-γ coincidence relationships. Specifically, a band previously given as an excited positive-parity band was reassigned as the "missing" signature partner of the known yrast negative-parity band. The first quasiproton alignment was observed for the first time in the favored positive- and negative-parity bands. A cluster of high-lying states was also explored and interpreted as three-quasiparticle states resulting from the coupling of a $g_{9/2}$ neutron to the lowest 5^-, 6^-, and 7^- states of the ^{70}Se core.

The lifetimes of 17 excited states were measured using the DSAM, with the experimental line shapes obtained at two separate detector angles and by gating from above the transitions of interest whenever possible. Three new lifetimes were measured in both favored signatures of the yrast positive- and

negative-parity bands, which were extended up to $(\frac{33}{2}^{+})$ and $(\frac{31}{2}^{-})$ states. Six lifetimes are now available in the unfavored bands. Transition quadrupole moments $|Q_t|$ inferred from the lifetimes indicate an intermediate degree of collectivity when compared with neighboring odd-A nuclei and demonstrate the transitional character of ^{71}Se between nuclei that show high collectivity and those which predominantly indicate single-particle excitations.

Total Routhian surfaces resulting from cranked Woods-Saxon calculations for all four observed bands indicate the features of shape competition and γ softness at low spin that is typical of $A \approx 70$ nuclei. At high spin, the calculations predict triaxial shapes with $\gamma > 0^{\circ}$ for both signatures of the lowest positive- and negative-parity configurations. Theoretical $|Q_t|$ values deduced from these calculations show better agreement with the experimental results for the positive-parity bands than for the negative-parity bands, although the theoretical values are quite sensitive to the value of the γ shape parameter used in the calculation.

ACKNOWLEDGMENTS

This work was supported in part by the US National Science Foundation through Grants No. PHY-04-56463 (FSU) and No. PHY-0648751 (OWU), as well as the Ohio Wesleyan University Summer Science Research Program. We thank W. Nazarewicz for providing the results of his cranked Woods-Saxon calculations and the staff of the FSU John D. Fox superconducting accelerator for their support throughout the experiment.

[1] W. Nazarewicz, in *High Spin Physics and Gamma-Soft Nuclei*, edited by J. X. Saladin, R. A. Sorensen, and C. M. Vincent (World Scientific, Singapore, 1991), p. 406.
[2] J. H. Hamilton, A. V. Ramayya, W. T. Pinkston, R. M. Ronningen, G. Garcia-Bermudez, H. K. Carter, R. L. Robinson, H. J. Kim, and R. O. Sayer, Phys. Rev. Lett. **32**, 239 (1974).
[3] J. Döring, G. D. Johns, M. A. Riley, S. L. Tabor, Y. Sun, and J. A. Sheikh, Phys. Rev. C **57**, 2912 (1998).
[4] S. M. Fischer, D. P. Balamuth, P. A. Hausladen, C. J. Lister, M. P. Carpenter, D. Seweryniak, and J. Schwartz, Phys. Rev. Lett. **84**, 4064 (2000).
[5] G. Rainovski *et al.*, J. Phys. G **28**, 2617 (2002).
[6] J. Ljungvall *et al.*, Phys. Rev. Lett. **100**, 102502 (2008).
[7] E. A. McCutchan, C. J. Lister, T. Ahn, R. J. Casperson, A. Heinz, G. Ilie, J. Qian, E. Williams, R. Winkler, and V. Werner, Phys. Rev. C **83**, 024310 (2011).
[8] J. Heese, K. P. Lieb, L. Lühmann, F. Raether, B. Wörmann, D. Alber, H. Grawe, J. Eberth, and T. Mylaeus, Z. Phys. A **325**, 45 (1986).
[9] A. M. Hurst *et al.*, Phys. Rev. Lett. **98**, 072501 (2007).
[10] A. Obertelli *et al.*, Phys. Rev. C **80**, 031304 (2009).
[11] I. Stefanescu *et al.*, Phys. Rev. C **69**, 034333 (2004).
[12] G. Mukherjee, P. Joshi, S. N. Roy, S. Datta, R. P. Singh, S. Muralithar, and R. K. Bhowmik, Z. Phys. A **359**, 111 (1997).
[13] R. Loritz *et al.*, Eur. Phys. J. A **6**, 257 (1999).
[14] E. Hagberg, J. C. Hardy, H. Schmeing, H. C. Evans, U. J. Schrewe, V. T. Koslowsky, K. S. Sharma, and E. T. H. Clifford, Nucl. Phys. A **383**, 109 (1982).
[15] *Table of Isotopes*, 7th ed., edited by C. M. Lederer and V. S. Shirley (Wiley-Interscience, New York, 1978).
[16] R. Duffait, A. Charvet, and R. Chery, Phys. Rev. C **17**, 2031 (1978).
[17] A. A. Alexandrov, M. P. Kudoyarov, I. Kh. Lemberg, and A. A. Pasternak, Nucl. Phys. A **321**, 189 (1979).
[18] J. Eberth, L. Cleemann, and N. Schmal, in *Proceedings of the International Symposium on In-Beam Nuclear Spectroscopy, Debrecen, Hungary, May 14–18, 1984*, edited by Zs. Dombradi and T. Fenyes (Akademiai Kiado, Budapest, 1984), p. 23.
[19] T. Heck, Ph.D. thesis, Universität zu Köln, 1983.
[20] A. V. Ramayya, Nucl. Instrum. Methods Phys. Res. B **40/41**, 432 (1989).
[21] J. Pavan, Ph.D. thesis, Florida State University, 2003.
[22] http://fsunuc.physics.fsu.edu/~caussyn/.
[23] E. F. Moore, P. D. Cottle, C. J. Gross, D. M. Headly, U. J. Hüttmeier, S. L. Tabor, and W. Nazarewicz, Phys. Rev. C **38**, 696 (1988).
[24] F. Kearns and J. N. Mo, Nucl. Data Sheets **27**, 517 (1979).
[25] F. Becker *et al.*, Nucl. Phys. A **626**, 799 (1997).
[26] R. S. Zighelboim, S. G. Buccino, F. E. Durham, J. Döring, P. D. Cottle, J. W. Holcomb, T. D. Johnson, S. L. Tabor, and P. C. Womble, Phys. Rev. C **50**, 716 (1994).
[27] N. Fotiades *et al.*, Phys. Rev. C **59**, 2919 (1999).
[28] R. A. Kaye *et al.*, Phys. Rev. C **83**, 044316 (2011).
[29] http://www.srim.org.
[30] G. Cowan, *Statistical Data Analysis* (Oxford University Press, New York, 1998).
[31] P. R. Bevington, *Data Reduction and Error Analysis for the Physical Sciences* (McGraw-Hill, New York, 1969).
[32] F. Cristancho and K. P. Lieb, Nucl. Phys. A **486**, 353 (1988).
[33] S. L. Tabor, J. Döring, J. W. Holcomb, G. D. Johns, T. D. Johnson, T. J. Petters, M. A. Riley, and P. C. Womble, Phys. Rev. C **49**, 730 (1994).
[34] F. Cristancho *et al.*, Nucl. Phys. A **501**, 118 (1989).
[35] http://www.nucleonica.net/wiki/index.php?title=Help%3A Range_%26_Stopping_Power.
[36] *Handbook of Nuclear Chemistry*, edited by A. Vértes, S. Nagy, and Z. Klencsár, Vol. 3 (Kluwer Academic, Dordrecht, 2003).
[37] M. Wiedeking *et al.*, Phys. Rev. C **62**, 024316 (2000).
[38] G. M. Gusinskii, V. S. Zvonov, I. Kh. Lemberg, and V. E. Mitroshin, Izv. Akad. Nauk SSSR, Ser. Fiz. **44**, 92 (1980).
[39] W. Nazarewicz, J. Dudek, R. Bengtsson, T. Bengtsson, and I. Ragnarsson, Nucl. Phys. A **435**, 397 (1985).
[40] S. M. Fischer and C. J. Lister, http://meetings.aps.org/link/BAPS.2010.DNP.NG.8.
[41] M. Wiosna, J. Busch, J. Eberth, M. Liebchen, T. Mylaeus, N. Schmal, R. Sefzig, S. Skoda, and W. Teichert, Phys. Lett. B **200**, 255 (1988).
[42] W. Nazarewicz, M. A. Riley, and J. D. Garrett, Nucl. Phys. A **512**, 61 (1990).
[43] J. Dudek, W. Nazarewicz, and P. Olanders, Nucl. Phys. A **420**, 285 (1984).
[44] I. Hamamoto and B. R. Mottelson, Phys. Lett. B **132**, 7 (1983).
[45] P. Ring, A. Hayashi, K. Hara, H. Emling, and E. Grosse, Phys. Lett. B **110**, 423 (1982).
[46] F. Johnston-Theasby *et al.*, Phys. Rev. C **78**, 034312 (2008).